D5.2

Demonstrations of smart connectivity platform, support for resilient applications, and novel technologies

Project number:	101013425
Project acronym:	**REINDEER**
Project title:	REsilient INteractive applications through hyper Diversity in Energy Efficient RadioWeaves technology
Project Start Date:	1st January 2021
Duration:	48 months
Programme:	H2020-ICT-52-2020
Deliverable Type:	Demonstrator (DEC)
Reference Number:	ICT-52-2020 / D5.2 / 0.00
Workpackage:	WP5
Due Date:	31st Dec, 2024
Actual Submission Date:	9th Dec, 2024
Responsible Organisation:	KU Leuven
Editor:	Gilles Callebaut
Dissemination Level:	PU
Revision:	0.00
Abstract:	This deliverable consolidates experimental findings from D5.1 and D5.3 into a series of demonstration videos, offering a visual representation of key challenges and solutions addressed in REINDEER. These videos cover topics such as dynamic resource allocation, robustness versus latency trade-offs, accurate positioning, energy-neutral device interaction, and multi-user capabilities. Together, they highlight the advancements in distributed antenna systems and wireless power transfer technologies, offering new insights into the development of next-generation wireless ecosystems.
Keywords:	RadioWeaves, validation, experiments, testbeds, energy-neutral devices

The REINDEER project has received funding from the European Union's Horizon 2020 research and innovation programme under grant agreement No 101013425.

Editor

Gilles Callebaut (KU Leuven)

Contributors

Gilles Callebaut, Jarne Van Mulders, Bert Cox, Liesbet Van der Perre (KU Leuven)

Liang Liu, Juan Vidal Alegría, Xuhong Li, Christian Nelson, William Tärneberg, Emma Fitzgerald, Fredrik Tufvesson, Yingjie Xu, Ove Edfors (ULund)

Benjamin J. B. Deutschmann, Thomas Wilding, Klaus Witrisal (TU Graz)

Koen Deforche (BlooLoc)

Ulrich Mühlmann (NXP)

Internal reviewers

Pål Frenger (EAB)
Marion Habernig (Technikon)

Executive Summary

This document, reporting on D5.2, presents the proof-of-concept developments from Task 5.1 and Task 5.2 of REINDEER, focusing on the smart connectivity platforms enabled by the RadioWeaves architecture. It validates resilient wireless applications in dynamic scenarios and explores interactions with energy-neutral devices, showcasing that improved service levels are achievable with practical implementation complexity. The deliverable consolidates experimental findings from D5.1 and D5.3 into demonstration videos that provide a visual overview of key challenges and solutions addressed in REINDEER.

The demonstration videos cover experiments on dynamic resource allocation, robustness versus latency trade-offs, accurate positioning, powering and communicating with energy-neutral devices, and multi-user capabilities. These experiments highlight trade-offs between performance, energy efficiency, and scalability while validating methods such as wireless power transfer and distributed antenna systems. By bridging gaps in current research, this deliverable underscores the potential of RadioWeaves systems in advancing next-generation wireless technologies and identifies challenges to address for real-world implementation. The videos are publicly available at: https://vimeo.com/showcase/reindeer-results-video-showcase.

Contents

Glossary

3D three-dimensional.

5G fifth-generation.

6G sixth-generation.

BER bit error rate.

CF cell-free.

CSI channel state information.

CSP contact service point.

DC direct current.

D-MIMO distributed MIMO.

DAQ data acquisition system.

DPC dirty-paper coding.

ECSP edge computing service point.

EN energy neutral.

END energy-neutral device.

EP energy profiler.

ESL electronic shelf label.

FD front-haul distance.

GPU graphical processing unit.

GSCM geometry-based stochastic model.

KPI key performance indicator.

LIS large intelligent surface.

LoS line-of-sight.

MIMO multiple-input multiple-output.

MRC maximum ratio combining.

NLoS non-line-of-sight.

NR New Radio.

OLoS obstructed-line-of-sight.

OOK on-off keying.

PEB positioning error bound.

PHY physical.

PL path loss.

PoE power-over-Ethernet.

PTP precision-time protocol.

RF radio frequency.

RF WPT radio frequency wireless power transmission.

RLS recursive least squares.

RMSE root-mean-square error.

RPi Raspberry Pi.

SDR software-defined radio.

SLAM simultaneous localization and mapping.

SMC specular multipath component.

SNR signal-to-noise ratio.

SVS singular value spread.

UE user equipment.

ULD uplink data.

ULP uplink pilot.

URA uniform rectangular array.

WPT wireless power transfer.

XL-MIMO extremely large-scale MIMO.

ZF zero-forcing.

Chapter 1

Introduction

This deliverable presents the proof-of-concept developments from Task 5.1 and Task 5.2 of REINDEER, showcasing the smart connectivity platforms enabled by the RadioWeaves architecture. It validates the functionality of resilient wireless applications in dynamic scenarios and demonstrates their interaction with energy-neutral devices. The deliverable highlights that these improvements in service levels are achievable with practical implementation complexity.

Relation to Other Deliverables

Although D5.2 is officially classified as a *Demonstrator*, this document is provided to consolidate and summarize the proof-of-concept achievements from REINDEER. D5.1 contained the experimental plans in REINDEER. The conducted experiments together with their description, methodologies, and experimental findings are provided in D5.3. These are distilled into demonstration videos in D5.2 and described here. These videos offer a concise and visual representation of the results disseminated in D5.3.

Demonstration Videos

The deliverable includes a description of a series of demonstration videos, each addressing specific challenges tackled in REINDEER. The videos cover:

1. Overview of testbeds, simulators, and experiments. (Chapter 2)
2. Experiment 1: Dynamic resource allocations via federations. (Chapter 3)
3. Experiment 2: Robustness versus latency trade-offs. (Chapter 4)
4. Experiment 3: Accurate positioning. (Chapter 5)
5. Experiment 4:
    a) Powering energy-neutral devices. (Chapter 6)
    b) Communicating with energy-neutral devices. (Chapter 7)
    c) Positioning energy-neutral devices. (Chapter 8)
6. Experiment 5: Multi-user capabilities. (Chapter 9)

These videos will be made publicly available on social media, the REINDEER website, and through the REINDEER results video showcase at:

https://vimeo.com/showcase/reindeer-results-video-showcase.

Deliverable Structure

The deliverable is organized as follows:

- Chapter 2 summarizes the testbeds, simulators, and experiments, including their contributions to various challenges.
- Chapters 3-9 describe each demonstration video, following a standardized format:
  - Aim of the demonstrator.
  - Key takeaways.
  - Experimental results and conclusions.
  - Video description.
  - References to published or submitted materials from the REINDEER consortium.

This document not only bridges the insights from previous tasks but also provides a clear and engaging format to disseminate the project's key findings to diverse audiences.

Chapter 2

Overview of Testbeds, Simulators and Experiments

An overview of the available testbeds, simulators and experiments used in the REINDEER are provided. The aim of this video is to illustrate the diverse set of resources developed in REINDEER. This overview is also provided in D5.1 and D5.3, where the key features and the main focus of different testbeds are summarized.

Table 2.1: Overview of the conducted experiments.

Num.	Experiments	KPIs	Testbeds	ENDs	Simulators
1	Dynamic resource allocations via federations	5, 13	LunCH		LuSim
2	Robustness versus latency trade-off	6, 7	LuLIS		LuSim
3	Accurate positioning	8	LARVA		TugSim
4	Powering, communicating with and positioning of ENDs				
4a	Powering ENDs	11	LARVA and Techtile	KUL EN and NXP EN	TugSim
4aa	Random-phased charging		Techtile	KUL EN and NXP EN	
4ab	Geometry-based WPT		LARVA and Techtile		
4ac	Reciprocity-based WPT		Techtile	KUL EN and NXP EN	
4b	Communicating with ENDs	9	Techtile	KUL EN and NXP EN	TugSim
4c	Positioning of ENDs	10	LARVA and Techtile	KUL EN	TugSim
5	Multi-user capabilities	1, 2	LunCH		LuSim

2.1 Simulators

2.1.1 TugSim

TugSim is a Matlab implementation of ray tracing to model specular multipath propagation developed by TUG, and is currently not publicly available. It was extended from a 2-dimensional ray tracing toolbox from TUG, with the main advantage being the flexibility to add and evaluate virtual sources during run time of algorithms, e.g., mutlipath-assisted positioning or simultaneous localization and mapping (SLAM) algorithms. The simulation framework allows to compute image source locations, termed virtual anchors (VAs), and enables simulation of realistic multipath channels to obtain spatially consistent channels. An exemplary virtual environment inf form of a floor plan is shown in Figure 2.1. Using the floor plan model with a predefined structure, it is possible to use the ray tracing methods to perform “online” updates of the floor plan during algorithm runtime. The extension to 3-dimensional ray tracing that was implemented during REINDEER was an important step to allow algorithm validation and development in realistic environments.

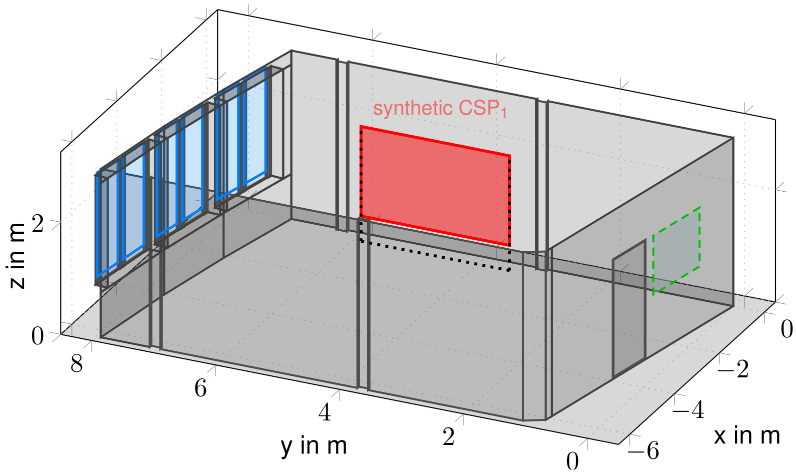

(a)

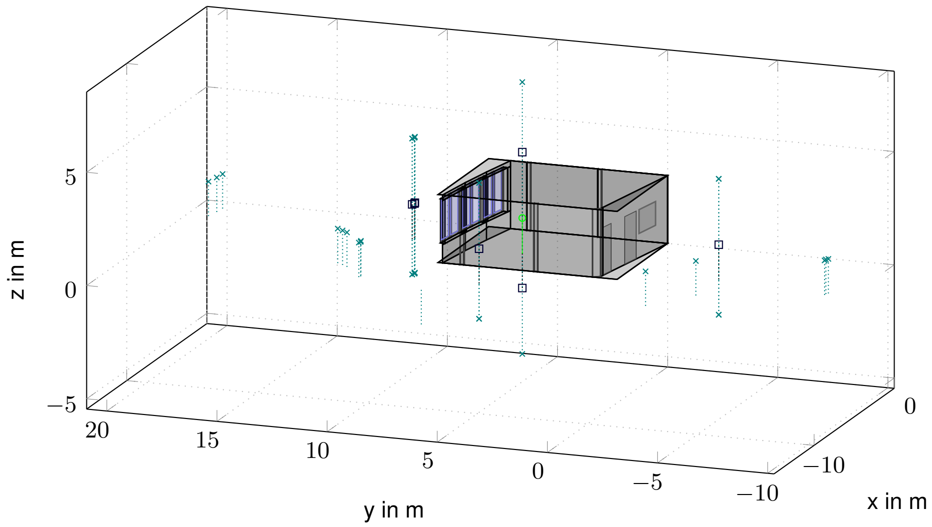

(b)

Figure 2.1: Overview of TugSim capabilities. (a) Scenario model of a medium-sized indoor environment, including different types of materials, including a measurement location used with the LARVA testbed (indicated as CSP$_1$), see Figure 2.5 on Page 8 for a photo. (b) shows first and second order image sources (black squares and teal $\times$ respectively) computed for an exemplary transmitter in the environment (green circle).

2.1.2 LUnitySim

Unlike traditional systems such as WiThRay [1], QuaDRiGa [2], [3], and NVIDIA Sionna [4], our simulator LUnitySim [5] integrates advanced geometry-based stochastic model (GSCM) and Exhaustive Ray Tracing methodologies. This integration allows for detailed and realistic simulations of wireless propagation in varied environments, from urban landscapes to indoor settings [6]–[10]. By leveraging the Unity game engine, the simulator efficiently handles complex ray-casting tasks, making use of graphical processing unit (GPU) capabilities to serve the growing needs of researchers and engineers in this field. Our simulator's architecture is designed for flexibility and scalability, with externalized configurations and scenario definitions through JSON or YAML files. This modular approach supports a wide range of applications, including large-scale studies and sensitivity analyses. Furthermore, the simulator extends beyond its predecessors by including fully 3D indoor and cell-free scenarios, accommodating a large number of antennas and supporting studies on dynamic resource allocation.

The cross-layer capabilities of our simulator facilitate a seamless interplay between the physical and application layers, enabling applications like resource orchestration and data synthesis for machine learning. This versatility ensures that the simulator remains a vital tool for exploring, developing, and deploying LuLIS-based sixth-generation (6G) networks.

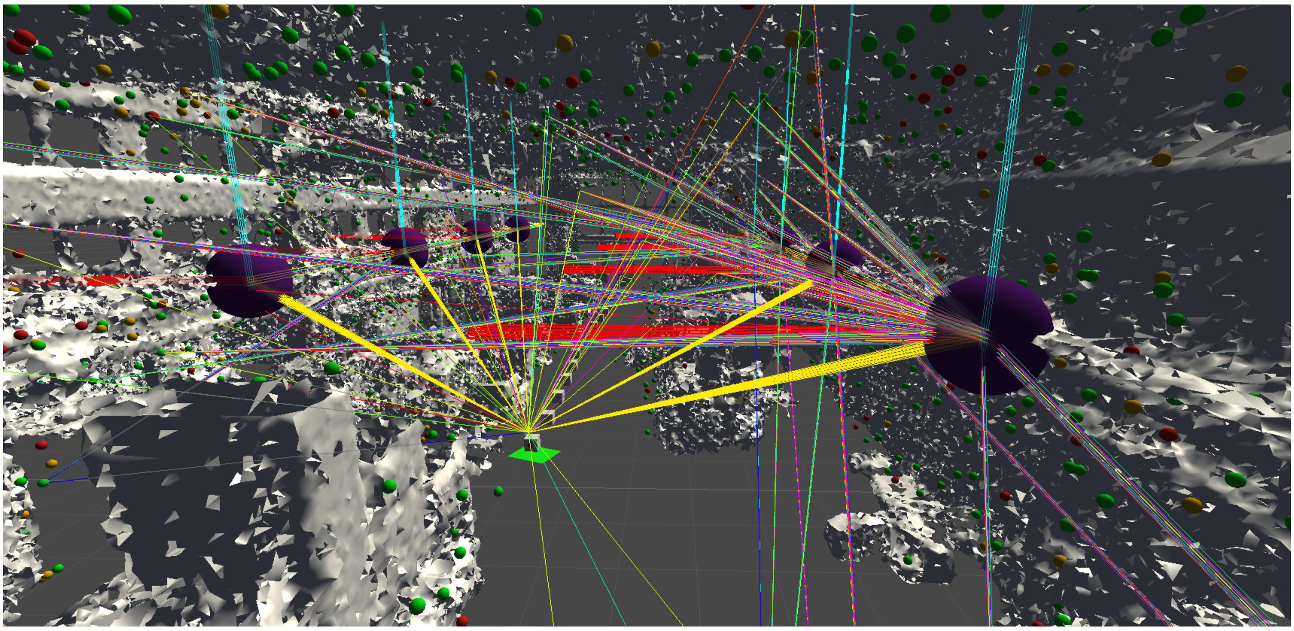

Figure 2.2: Screenshot and example of LUnitySim visualization.

2.1.3 LUSim

LUsim is a system-level simulation platform designed to evaluate and optimize resource allocation algorithms within the RadioWeaves infrastructure. Developed by [11] and extended by [12]. Unlike the LUnitySim radio channel simulator, which focuses on detailed modeling of physical-layer interactions such as path loss, fading, and interference, the system-level simulator emphasizes the broader network dynamics and resource management strategies.

LUsim models the interactions among user equipments (UEs), contact service points (CSPs), and edge computing service points (ECSPs), providing a comprehensive framework for analyzing system-wide performance under varying conditions. It supports simulations of user behaviors, mobility, and dynamic resource allocation, enabling researchers to explore the impact of high-level decisions on key metrics such as latency, throughput, and utility.

Key capabilities include:

- **System Dynamics Modeling**: Simulation of large-scale network interactions, including user mobility, federation formation, and dynamic resource allocation.
- **Algorithm Evaluation**: Implementation and testing of resource allocation strategies at the system level, focusing on network-wide performance metrics rather than individual link-level characteristics.
- **Realistic Network Environment**: Incorporation of topologies such as lattice, daisy-chain, and tree structures to simulate diverse operational scenarios.

- **Visualization and Analysis Tools**: A three-dimensional (3D) interface to visualize network layouts, user movements, and resource allocation dynamics, providing actionable insights for optimization.

By operating at the system level, LUsim complements the detailed physical-layer simulations of the LUnitySim radio channel simulator, offering a holistic approach to evaluating and refining RadioWeaves infrastructure. This dual-layer simulation framework ensures that both macro-level strategies and micro-level interactions are rigorously assessed, enabling the development of robust and efficient solutions for next-generation wireless systems.

2.2 Testbeds

2.2.1 Techtile

The measurement facility and RadioWeaves approach, Techtile [13], [14] (Figure 2.3), is an open, both in design and operation, and unique testbed to evaluate the newly envisioned systems in REINDEER. Although Techtile was under construction prior to the REINDEER project, the implementation and experiments were made possible and done in REINDEER.

Contact person: Gilles Callebaut `gilles.callebaut@kuleuven.be`
Code and documentation: `github.com/techtile-by-dramco`

Figure 2.3: REINDEER consortium in Techtile to illustrate the scale of the room.

Support Structure. The Techtile testbed comprises a modular wooden support structure with 140 detachable tiles (Figure 2.4). It features an Ethernet-based backbone for power, data, and synchronization. Tiles accommodate sensors, actuators, transmitters, receivers, and processing resources, providing a flexible platform for research in areas like communication, sensor fusion, and distributed computing.

Construction. Based on the WikiHouse concept, the structure includes walls, ceiling, and floor supporting 28, 42, and 52 tiles, respectively. Each tile measures $120\,\mathrm{cm}$ by $60\,\mathrm{cm}$, providing modularity for flexible deployment.

Ethernet-Based Backbone. The backbone integrates a central server and Ethernet switches with power-over-Ethernet (PoE), supporting IEEE-1588 precision-time protocol (PTP) for sub-microsecond clock synchronization. A $9\,\mathrm{kW}$ PoE budget powers tiles, enabling scalability and emulation of network topologies.

Central Processing and Networking. The central server features $512\,\mathrm{GB}$ RAM, GPUs, and CPUs. Networking is managed with Dell switches supporting high-speed Ethernet and IEEE 1588v2 synchronization.

Synchronization. Synchronization options include:

Ethernet-based: IEEE 1588v2 for scalable synchronization.

Dedicated cabling: High-accuracy baseline using clock distribution modules.

Over-the-air: Supports calibration and synchronization research for distributed systems.

Data Acquisition System. A data acquisition system (DAQ) system with synchronized channels provides high-resolution data acquisition ($1.25\,\mathrm{MS/s}$) and actuator control ($3.3\,\mathrm{MS/s}$), supporting sensor fusion and multi-modal sensing.

On-Tile Components. Each tile hosts:

- A custom PoE board for power management.
- software-defined radios (SDRs) for RF communication, connected to Raspberry Pi (RPi) 4.
- Local and central processing for edge and cloud computing research.

Interface and Data Exchange. Users interact via open-source tools, with a documented workflow available at `github.com/techtile-by-dramco`. Data is stored and processed centrally for reproducibility and validation.

Figure 2.4: Left: The Techtile support structure – Right: The back of three tiles, equipped with the default setup, i.e., a software-defined radio (USRP B210), 2 antennas, a processing unit (Raspberry Pi 4) and power supply with Power-over-Ethernet. Each tile is connected to the central unit with an Ethernet cable, providing both power and data.

2.2.2 LARVA

The **LAR**ge **V**irtual **A**rray (LARVA) measurement testbed was developed by Graz University of Technology for REINDEER to perform measurements with arrays of arbitrary geometry. Using a virtual array allows to obtain "ideal", or fully calibrated arrays of arbitrary aperture. This allows validation of super resolution channel estimation algorithms, positioning algorithms or environment sensing. The measurement testbed consists of two positioning devices that contain two linear axes to position an antenna at an arbitrary location in the measurement area. The measurement area spans roughly 2.5×1.5 meters maximum. RF measurements can be performed with any hardware that can be mounted on the movable sledge. A photo of one of the virtual arrays mounted on a wall in a measurement environment is shown in Figure 2.5. The main limiting factor when performing measurements of arrays will be due to the requirement of stationarity during the full measurement duration, e.g., the measurement environment should not change during recording data for one full virtual array. With the flexibility of forming arbitrary geometry virtual arrays, it will be an important measurement system for future measurement campaigns. In addition to LARVA, smaller positioning devices are in use at TUG to extend the capabilities of LARVA to multiple-input multiple-output (MIMO) scenarios (with a reasonable number of antennas). These smaller devices are also used in teaching activities to allow students to obtain firsthand experience with spatial measurements.

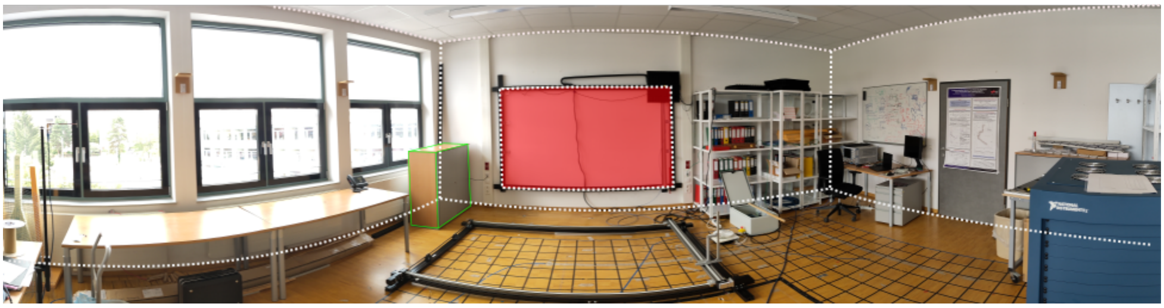

Figure 2.5: Photo of one of the positioning devices of LARVA mounted on a wall. The measurement location is also highlighted in the TugSim scenario shown in Figure 2.1.

2.2.3 LuLIS

LuLIS (Lund University Large Intelligent Surface testbed) is a distributed and modular testbed, where CSPs of 16-antenna arrays with localized processing capabilities are distributed in the environment and together operate coherently with a bandwidth of $100\,\mathrm{MHz}$ in the $3.7\,\mathrm{GHz}$ band. Each CSP is equipped with an AMD/Xilinx RFSoC device (more specifically, Zynq UltraScale+ RFSoC ZCU216 Evaluation Kit, shown in Figure 2.6b). ZCU216 integrates 16 ADCs/DACs that can do direct RF-sampling up to 6GHz. The corresponding logic cells, DSP slices, and memory enable real-time processing for distributed MIMO (D-MIMO) systems. It also features 100G-Ethernet enabling high-throughput data shuffling between CSPs. Based on RFSoC technology, the testbed is software controlled and supports real-time distributed processing, making it capable of both exploring many different service types, such as communication and positioning and also performing propagation measurements for the purpose of channel modeling, sensing and creation of datasets for machine-learning experiment.

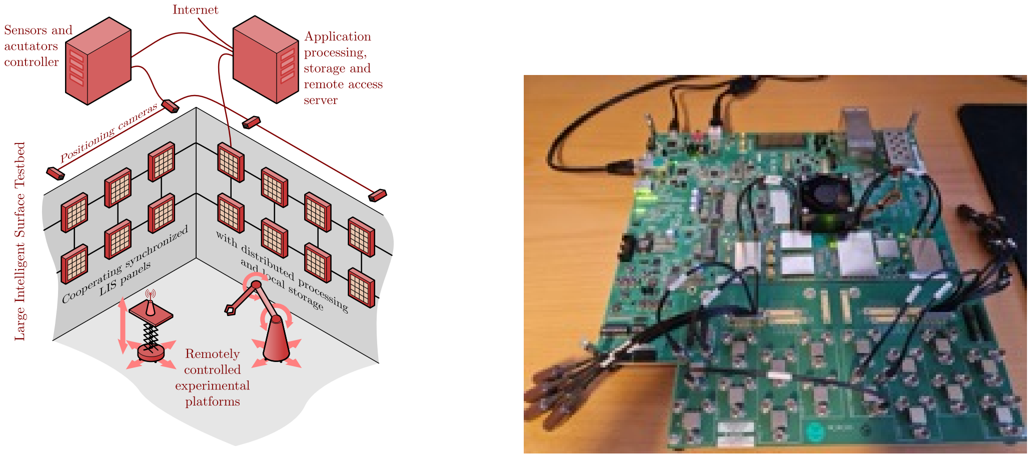

(a) (b)

Figure 2.6: (a) large intelligent surface (LIS) testbed under development at Lund University (LuLIS). Cooperating synchronized CSPs (b) The AMD/Xilinx ZCu216 RFSoC board, which is the main processing unit for LIS testbed CSPs.

2.2.4 LunCH

LunCH is a group of channel sounders that are used to evaluate different properties of the RadioWeaves channel and its multi-user capabilities. It comprises three different channel sounders that have been used in experiments: RUSK Lund, a distributed MIMO channel sounder [15], and a switched wideband distributed MIMO sounder [16]. RUSK Lund is a wideband MIMO channel sounder, initially used to capture the RadioWeave channel properties and multi-user separability [17]. Using a virtual array technique, it is possible to measure the transfer functions from 16 simultaneous users to virtual walls of antennas, i.e., the RadioWeave, consisting of several thousands of antennas ($15\,520$ patch antennas in [17]). For dynamic analysis and positioning experiments, we have used a distributed MIMO channel sounder set-up [15], which then culminated in the wideband distributed MIMO sounder [16] using the CSPs concept. The latter sounder enables wideband dynamic experiments with 4 CSPs, each comprising 2 panels with a total of 32 antenna ports (16 dual-polarized patch arrays). The photos of the BS-side panel and UE-side robot are shown in Figure 2.7. Multiuser capabilities are evaluated virtually, though it is also possible to have up to 16 simultaneous (switched at sub-ms level) users.

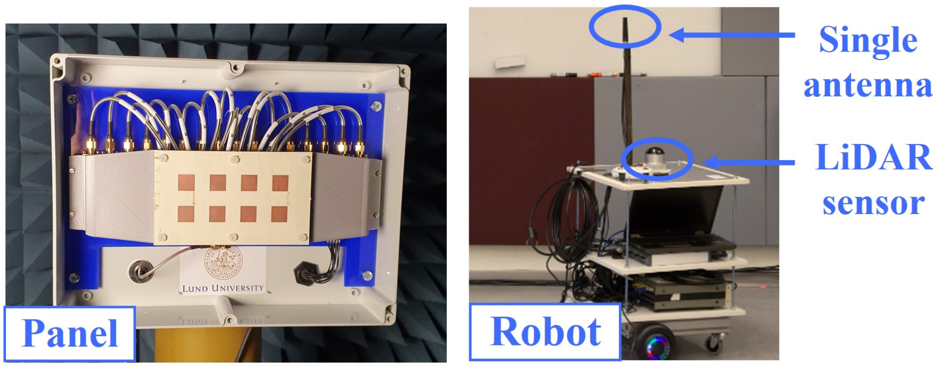

(a) (b)

Figure 2.7: Photos of (a) the panel used at the BS side and (b) robot at the UE side.

2.3 Testbed and Simulator Usage in Experiments

Figure 2.8 (also in D5.3) illustrates how these REINDEER-related testbeds and simulators are used for different experiments detailed in D5.3. Many experiments combine features abstracted from Level 3/4 testbed [18] with simulators for analyzing the trade-offs in different scenarios. As an example, experiment 2 embeds the real-life hardware implementation latency from LuLIS in LUnitySim to evaluate the robustness versus latency trade-offs for different RadioWeaves deployment scenarios.

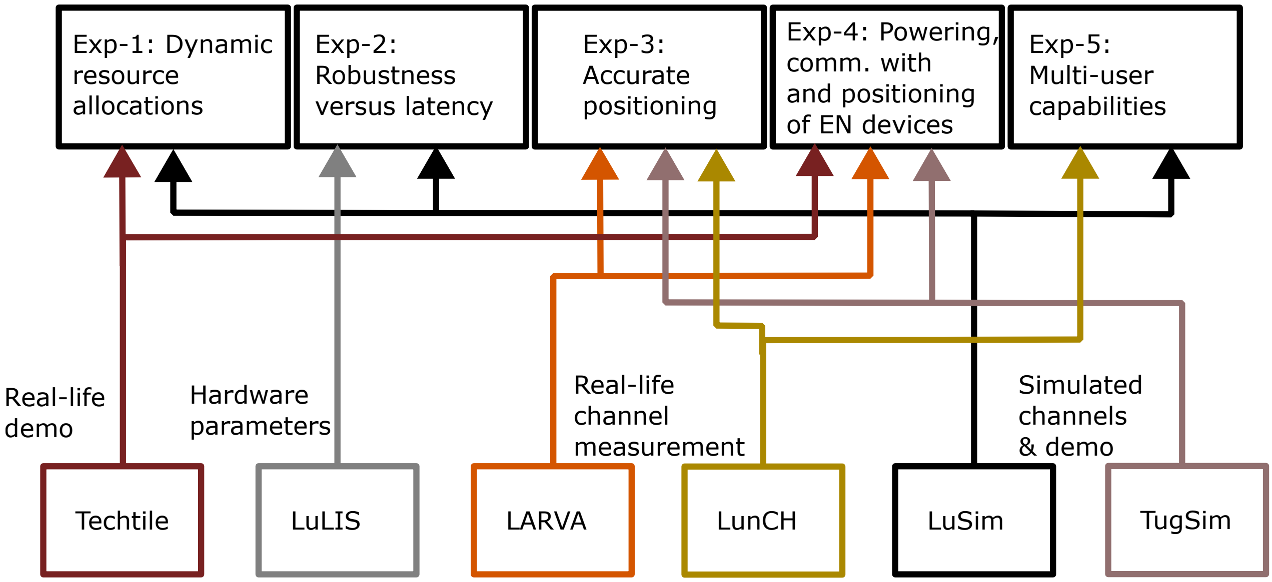

Figure 2.8: Overview of how testbeds and simulators contribute to different experiments.

Chapter 3

Experiment 1. Dynamic resource allocations via federations

3.1 Description

Due to the diverse set of services in modern wireless networks, resource allocation, including processing and radio elements, must be tailored to the specific requirements of each application. For example, wireless power transfer benefits from allocating charging resources near the intended device to maximize efficiency. Conversely, XR applications require high spatial diversity of antenna resources to mitigate outages and latency peaks caused by user mobility and head movement. These varying demands highlight the need for dynamically grouping resources, both temporally and spatially, within a cell-free context.

In REINDEER, we introduced the concept of *federation(s)* to represent a group of resources collaboratively serving a specific application. This demo aims to showcase the dynamic operation of federations through video demonstrations that align with the experiments conducted on throughput, precoding, topologies, federations, optimization, and energy usage. The demo provides a visualization of how federations adapt in real-time to changing network and application requirements.

3.2 Aim of the Demonstrator

The aim is to illustrate the following components:

- **Video of Ray Tracing in the M-Building at Lund University:** Using LUnitySim, this video visualizes the propagation environment within the M-building at Lund University, an industrial hall measuring 30 m × 11 m × 8 m. The hall, characterized by heavy metallic machinery, includes 12 CSPs distributed 4 m apart along a central axis at a height of 3.5 m, as described in [15]. These measurements were recreated in LUnitySim, as detailed in [5], to study the spatial dynamics of wireless communications and their impact on federation behavior. The video highlights how signals interact with the metallic environment and adapt to real-time federation requirements, as shown in Figure 2.2, which presents a snapshot of the simulation and the modeled M-building. To extend the original measurements, the simulations instantiate multiple UEs along the path of the measured UE, testing various topologies with differing numbers of CSPs and antenna configurations. Path loss is sampled every 100 ms and replicated in time to improve computational efficiency while enabling dynamic federation assignments. This approach demonstrates how federations adapt spatially and temporally to optimize resource allocation and performance, providing critical insights into the impact of wireless propagation on federation behavior in realistic industrial scenarios.

- **Federation Association Over Time:** The dynamic association of CSPs and UEs to federations over time will be illustrated. This will include insights into the impact of topologies, such as centralized and distributed configurations, on federation stability and performance.
- **Energy Usage and Federation Optimization:** The real-time operation of federations, focusing on energy usage optimization, will be shown. This component will highlight how energy is managed dynamically across different topologies and precoding strategies to balance efficiency and throughput.

3.3 Takeaway Points

The demo builds on the findings from the experiments, emphasizing the trade-offs between energy consumption, throughput, and user performance under varying topologies and precoding strategies. For example, federations are shown adapting to optimize throughput for distributed topologies or minimizing energy consumption in centralized configurations. Additionally, the visualizations demonstrate how dynamic federation orchestration supports resilient, real-time wireless applications, enabling adaptive responses to changing user and environmental conditions.

3.4 Conclusion

This demo serves as a demonstrator for D5.2, showcasing the near-real-time operation of federations, including their creation, movement, shrinking, and expansion, based on physical (PHY) layer conditions. It encapsulates the core aspects of throughput optimization, energy efficiency, and federation dynamics, providing a compelling visualization of the system's capabilities.

3.5 References

- **Measurements:** C. Nelson, X. Li, A. Fedorov, B. Deutschmann, and F. Tufvesson, "Distributed MIMO Measurements for Integrated Communication and Sensing in an Industrial Environment," *Sensors*, vol. 24, no. 5, p. 1385, Feb. 2024, ISSN: 1424-8220. DOI: `10.3390/s24051385`. [Online]. Available: `http://dx.doi.org/10.3390/s24051385` [15]
- **Federations: 9833918 9833918**
- **Optimization:** O. T. Demir, L. Méndez-Monsanto, N. Bastianello, E. Fitzgerald, and G. Callebaut, "Energy Reduction in Cell-Free Massive MIMO through Fine-Grained Resource Management," in *2024 Joint European Conference on Networks and Communications & 6G Summit (EuCNC/6G Summit)*, 2024, pp. 547–552. DOI: `10.1109/EuCNC/6GSummit60053.2024.10597081` [19]
- **Simulator:** W. Tärneberg, A. Fedorov, G. Callebaut, L. Van der Perre, and E. Fitzgerald, "Towards Practical Cell-Free 6G Network Deployments: An Open-Source End-to-End Ray

Tracing Simulator," in *2023 57th Asilomar Conference on Signals, Systems, and Computers*, 2023, pp. 1000–1005. DOI: 10.1109/IEEECONF59524.2023.10476998 [5]

Chapter 4

Experiment 2. Robustness versus latency trade-off

4.1 Description

The performance results will be evaluated using a simulated indoor scenario, while the latency results will consider real data from the LuLIS testbed. We will consider a uniform user distribution throughout the scenario under different user densities. The CSPs will be distributed along a horizontal line at the top of each of the two main walls, i.e., the walls covering the largest room dimension. Thus, each CSP would be facing another CSP at the opposite wall. We will consider different number of CSPs, as well as different number of CSP antennas such that we can compare the results of distributing versus concentrating antennas. Specifically, we will address both the case of having a fixed number of antennas distributed into a varying number of CSPs, as well as the case of changing the total number of antennas by changing the number of CSPs with fixed number of antennas per CSP. This way we may evaluate desirable deployment strategies, as well as overall system scalability. The focus will be put on CSPs consisting of square antenna arrays, which favors integrability and deployment. However, we will briefly explore some scenarios based on rectangular arrays to assess the impact of having different spatial resolutions for the vertical and horizontal axes.

4.2 Aim of the Demonstrator

Adding more CSPs with interference cancellation algorithms to provide more robust services could potentially reduce latency by avoiding retransmissions. On the other hand, more CSPs imply increased latency in coherence processing, *e.g.*, for zero-forcing (ZF) precoding and detection. As discussed in [20], [21], the processing latency depends on selected signal processing algorithms, the topology that connects CSPs, and also the deployment scenarios. For instance, the processing latency increases linearly with the number of CSPs when the recursive least squares (RLS) algorithm is mapped to a Daisy-Chain topology. Moreover, information exchange between CSPs with large front-haul distance (FD) may require multi-hop routing, which will result in much greater latency. An interesting aspect to be considered is that further increasing the number of CSPs may allow the use of local-processing-only algorithms, *e.g.*, maximum ratio combining (MRC), which will significantly reduce processing latency by parallel processing that minimizes the information exchange between CSPs. In summary, there is a non-trivial trade-off between the robustness and latency when changing the number of CSPs in service. Real-life hardware parameters from LuLIS, *e.g.*, processing and information exchange latency, will be used for calibrated simulation.

4.3 Video description

The video will start by presenting a preliminary schematic of the LuLIS system, together with some facts on the assumptions/considerations taken for the experiment. It will then superpose the considered frame structure and illustrate the definition of latency considered in this experiment.

The algorithmic part will be showcased by an animation showing how the decentralized processing data is accumulated throughout the network. To this end, a Daisy chain topology will be illustrated, together with the frame structure on the side. The different parts of the frame structure will be highlighted: at uplink pilot (ULP) the respective channel vectors will show up at the nodes, at uplink data (ULD) the respective received vectors will show up at each node, followed by the locally-processed ones. The sequential sum of the contributions will be then illustrated, showing the available aggregated data contributions at each node after each jump. A different animation will be performed for MRC and ZF to be able to compare the two approaches.

The final part of the video will show an animation jumping between different configurations of the simplified indoor scenario as illustrated in Fig. 4.1 [22], which depicts a $30\mathrm{m} \times 20\mathrm{m}$ industrial complex with random user distribution and CSPs distributed throughout the two longest walls. For each configuration, the reported latency, as well as the respective spectral efficiency, will be highlighted below for both MRC and ZF processing. Some final conclusions will be added in the end.

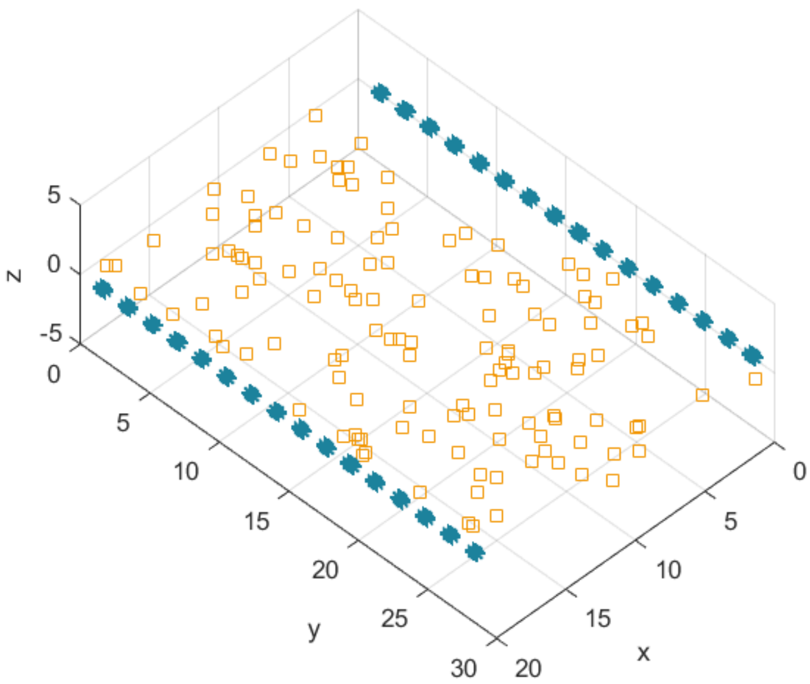

Figure 4.1: Example scenarios used in the spectral efficiency simulations. $P = 32$ with 8×4 CSPs.

Chapter 5

Experiment 3. Accurate positioning

A RadioWeaves infrastructure holds the potential for accurate positioning. RadioWeaves panels benefit from very large apertures, giving them high *angular resolutions*. The *range resolution* per panel suffers from a low bandwidth, but profits from the wide spatial distribution. However, multiple distributed RadioWeaves panels can cooperatively recover a great "range resolution", and a low positioning error bound (PEB) in general, as we demonstrated in [23].

The REINDEER consortium developed positioning bounds and algorithms in the deliverable D3.3 [24] and validates these in D5.3 based on measurements. A particular focus lies on the implementation of robust algorithms that will enable *resilient* communication and power transfer. We anticipate to evaluate the enhancement of robustness to the positioning through either in the implemented simulation and measurement testbeds, or also the BlooLoc positioning engine. While the former are specifically modeled according to the RadioWeaves infrastructure, the latter software is ideally suited to model imperfections of raw positioning sensor data to achieve robust positioning. To that extent, one needs to model the possible uncertainty/unreliability of the underlying sensors in a likelihood model for that specific sensor, and such models can be readily plugged into the positioning engine as well as the implemented testbeds.

5.1 Video Description

Two videos visualize how positioning, environment learning and tracking intersect seamlessly and ultimately support robustness in position-related applications.

Validation of performance bounds and environment learning.

This video will highlight the capabilities of physically large array when it comes to positioning of single antenna devices. We will visualize how the separation of the large array into subarrays decomposes the non-stationary channel received over the full array into different multipath components. Assuming the device to be, for simplicity, in line-of-sight (LoS) allows to use the estimated components directly to estimate the device location, i.e., without the need of performing multipath-based positioning by exploiting learned or prior available environment information. Using a two-step approach, we show the visualize the achievable positioning accuracy compares with the accuracy bounds derived in D3.3 [24].

Furthermore, after positioning of the device, the employed approach enables estimation of environment information in terms of calibrating the employed mirror source model. The estimates of the physical position of the UE will be used to obtain the virtual UE locations. The video will highlight how propagation between the (sub)arrays and the estimated sources contains information about the environment.

Environment-awareness for positioning and tracking.

The second video will highlight how a direct positioning approach based on the subarray decomposition of the physically large array estimate environment information based on measurement data.

Using our D-MIMO experiment [15], [25], [26], we have demonstrated that **distributed** radio infrastructures provide inherent **resilience** against **multipath fading** and **obstructions**. In the experiment, a mobile device moved through a harsh industrial environment and transmits uplink pilots. Twelve distributed single-antenna anchors acquired noisy channel estimates. To compensate for a lacking phase calibration at the anchors, we leveraged delay-Doppler direct positioning to estimate the position and velocity of the moving device directly at the radio signal (i.e., the noisy channels). We employed Bayesian state filtering, approximately implemented using a particle filter, to fuse the data received by the twelve anchors. Despite severe multipath propagation and obstructions through machinery in the environment, as well as a limited bandwidth of only $35\,\mathrm{MHz}$, we achieved near centimeter-level positioning accuracy.[1] Using only a simple LoS delay-Doppler channel model, this was possible in such a harsh scenario because the distributed infrastructure allowed to have at least some anchors in LoS conditions at all times.[2]

Using our extremely large-scale MIMO (XL-MIMO) experiment [27], we showed that **environment learning** (i.e., mapping) can aid a radio infrastructure to provide resilience against total OLoS conditions through **bypassing** the **obstructed LoS channel** by intentionally **exploiting multipath channels**, predicted through the inferred environment geometry. In this experiment, we again had a device that moved on a trajectory in a hallway from LoS conditions in front of a shelf to OLoS conditions behind a shelf, while transmitting uplink pilots. Fifteen closely located RadioWeaves panels (i.e., the "anchors"), each equipped with a (8×8) uniform rectangular array (URA) acquired noisy channel estimates. In this work, we leveraged angular-delay direct SLAM to estimate the position of the moving device simultaneously with the position and orientation of two walls in the hallway. We again employed Bayesian state filtering, approximately implemented using a particle filter, to fuse the data received by the fifteen anchors. An example of the likelihood function at one trajectory location is shown in Figure 5.1.
Using parametric *channel estimation*, we achieve a planar device position RMSE of around $6.5\,\mathrm{cm}$ at a low input signal-to-noise ratio (SNR) of $\leq -3\,\mathrm{dB}$ in LoS conditions and an RMSE of around $5.5\,\mathrm{cm}$ at a high input SNR of $\leq 30\,\mathrm{dB}$, both operating at the fifth-generation (5G) New Radio (NR) band n78 with a center frequency of $3.55\,\mathrm{GHz}$ and a bandwidth of $B = 500\,\mathrm{MHz}$ [28]. This *robustness* was achievable despite total OLoS conditions because the RadioWeaves infrastructure was able to correctly infer the environment geometry and position the UE solely via multipath channels, i.e., reflections via the estimated walls.
Using *channel prediction*, we leverage the position and environment geometry estimates to predict channel state information (CSI), i.e, for geometry-based multipath beamforming. Our algorithm provides a holistic closed-loop framework for iterative channel estimation and -prediction

[1]This relates to the planar position root-mean-square error (RMSE) (in the xy-plane), although we estimated the 3D position.
[2]In total obstructed-line-of-sight (OLoS) conditions, the RMSE increased to $49.3\,\mathrm{cm}$.

where the incorporated *physics-based knowledge* (a geometric channel model and state-space motion model for predicting the device position) helps to improve CSI in scenarios where the input SNR is low. Compared with a reciprocity-based beamformer, we showed that in the case of a low input SNR of $\leq -3\,\mathrm{dB}$, we can improve the *efficiency* (through the beamforming gain) with our geometry-based beamformer (leveraging predicted CSI) by a factor of up to $5\,\mathrm{dB}$, which provides 3.16 times more efficient power transfer in a wireless power transfer (WPT) context and likewise data rates improved up to 3.16 times the channel capacity, depending on the output SNR. We have further shown that using our motion model capable of predicting the future device position, we can likewise predict CSI multiple (even non-integer steps) into the future, which provides *high mobility support* if the pilot rate at the device cannot keep up with providing measured CSI for a reciprocity-beamformer possibly suffering severe losses given outdated CSI of a quickly moving device.

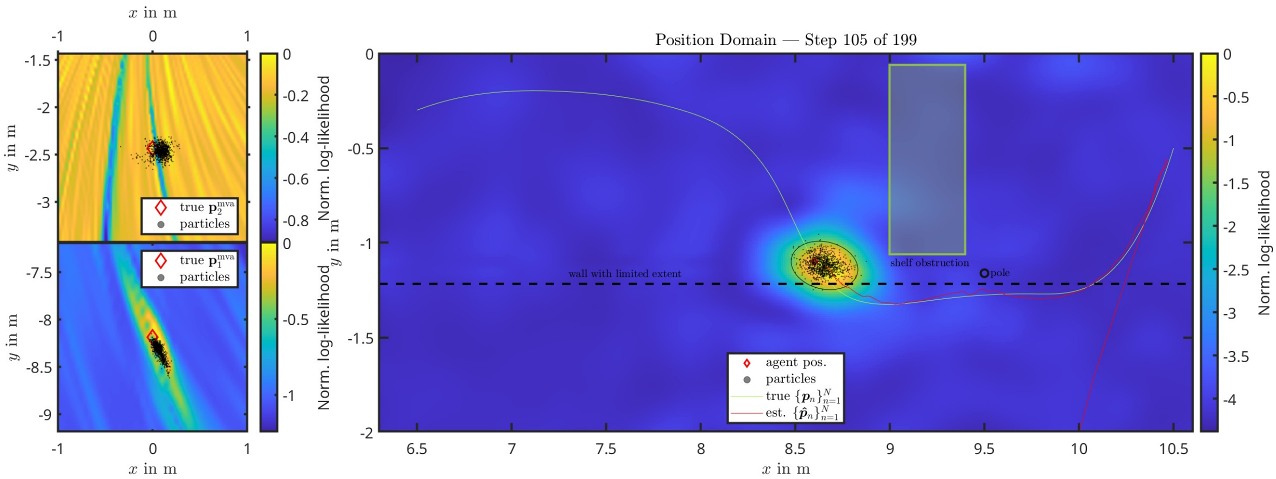

Figure 5.1: Example of geometry-based environment learning along a trajectory using measurement data, taken from D5.3 [27]. The likelihood function is plotted over a grid in the horizontal plane of the device trajectory (right), showing the maximum corresponding to the location of the device. The likelihood around environment features (representing two walls) is evaluated on the left.

Chapter 6

Experiment 4a. Powering energy-neutral device (END)

In a Radioweave architecture, a large number of resources—and consequently, antennas—are available to provide various services to end users. New opportunities arise, such as the ability for multiple CSPs to collaborate synchronously in supporting distributed radio frequency wireless power transmission (RF WPT). The REINDEER consortium has demonstrated, through mathematical analysis, simulations, and measurement campaigns, that power spots can be created, significantly improving the traditionally very low efficiency of RF WPT implementations. Various techniques have been explored to construct these spots. Additionally, hardware was developed to convert the captured RF energy into DC energy, providing a realistic perspective on the potential future applications.

6.1 Description

A video has been created to showcase the wireless powering of ENDs using the Techtile testbed, which was developed as part of the REINDEER project at KU Leuven. In this video, we demonstrate our Techtile infrastructure and showcase devices designed to perform automated measurements and demonstrate that constructive interference can be achieved at a specific location in the room. In Techtile, up to 84 distributed antennas are activated to demonstrate strategies such as beamforming and random-phase techniques.

In an earlier deliverable, the ESL use case was identified as a challenging scenario for distributed RF wireless power transfer (RFWPT). Therefore, in addition to demonstrating the investigated WPT strategies, the demonstrator showcases the charging of an electronic shelf label (ESL) to update its display without the use of batteries. The proof-of-concept is illustrated in Figure 6.1b.

In the following sections, we clarify the objectives of the demonstrator, highlight the key takeaway points, present the experimental results in an illustrative manner, provide a description of the video's progression, and conclude with our insights on this demonstration.

6.2 Aim of the Demonstrator

The goal of the demonstrator is to showcase the infrastructure and its role in experimental research. Techtile is designed to explore next-generation technologies for communication, sensing, and WPT, with a specific focus on the latter using primarily the ceiling tiles. This demonstrator introduces methods for measuring and investigating energy transfer efficiency. To achieve this, an energy profiler (EP) was developed to measure not only the radio frequency (RF) power but also the direct current (DC) power at the END. It is only the DC energy that is usable to power a specific application, and as explained in the video, this RF-to-DC conversion is associated with losses. Achieving a conversion efficiency higher than 50 percent is very difficult to realize. The design of the energy profiler is illustrated in Figure 6.1a.

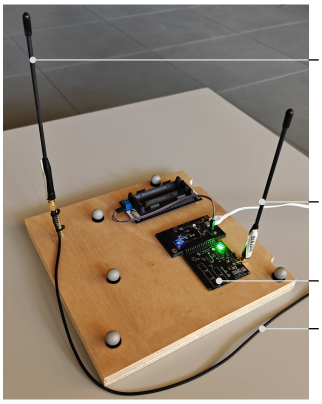

(a) Energy profiler (EP) design to measure DC power in real time.

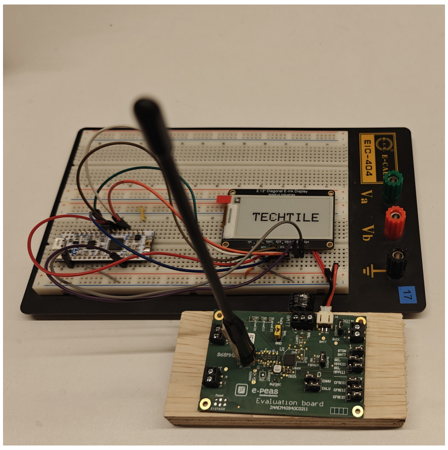

(b) Energy neutral (EN) electronic shelf label (ESL) device under development.

Figure 6.1: Overview of experimental setups.

The ceiling antennas of the Techtile infrastructure can be controlled in various ways. We showcase multiple RF WPT strategies to provide power to an END. These strategies include coherent solutions with techniques such as geometry-based and reciprocity-based beamforming. For situations where the location is unknown (making geometry-based beamforming impossible) or the END lacks the energy to send a pilot signal (making reciprocity-based beamforming impossible), a non-coherent solution using random-phase sweeping was explored. This technology spreads the power across the entire room and ensures the delivery of a small amount of wake-up energy to the ENDs. As a result, the energy densities and efficiencies are significantly lower than those of the coherent strategies.

6.3 Takeaway Points

Some key achievements from Experiment 4a are clarified here. Previous deliverables have shown that multiple applications are suitable for development as battery-free and energy-neutral solutions. However, the specifications of each application vary, and dedicated engineering is required to design ENDs effectively.

The energy available at the END depends on the transmission power, the number of antennas, the radiation pattern of the antennas, and the level of synchronization. The latter determines whether coherent strategies can be supported or not. The strategies are briefly explained below:

1. **Reciprocity-based WPT:** Enables precise beamforming after the device sends a pilot signal. For this, the device must have an initial amount of energy to perform this task.
2. **Geometry-based WPT:** Predict CSI using known geometry and align array phases. Effective when device positions are known, but adds complexity when they are unknown.
3. **Random-phase WPT:** Used for initial charging without requiring positional knowledge or phase calibration. It creates sufficient power fluctuations for the device to wake-up.

This experiment has provided valuable research insights into the achievable power levels at the END site and highlighted the differences in efficiency and power densities between strategies.

6.4 Experimental Results

The REINDEER consortium demonstrated that random-phase sweeping successfully induced power fluctuations sufficient to wake up devices. Furthermore, geometry-based beamforming was shown to achieve focused energy delivery by leveraging environmental knowledge for improved accuracy. Notably, increasing the order of the specular multipath components (SMCs) enhances the accuracy of the created power spot, though the specific improvement in accuracy remains to be quantified. Additionally, reciprocity-based WPT was validated under near-field conditions by using uplink pilots for coherent phase alignment. A snapshot of the recorded heatmaps of the received DC power for different WPT strategies is illustrated in Figure 6.2.

6.5 Video description

The video explores the process of WPT to ENDs, addressing key research questions through detailed demonstrations. It begins by introducing the Techtile testbed, highlighting its role in enabling WPT and experimental studies. The video then delves into methods for studying energy transfer efficiency, showcasing RF energy measurements recorded by a spectrum analyzer and precise DC power measurements using a custom-developed energy profiler (Figure 6.3), designed to account for nonlinearities and threshold voltage levels.

Next, the video illustrates how power is delivered to ENDs by visualizing strategies such as random-phase sweeping, geometry-based, and reciprocity-based beamforming. Dynamic animations of signal reflections within the Techtile environment demonstrate how these strategies function in real-world scenarios. Finally, the results of these strategies are presented through recorded heatmaps (Figure 6.2), emphasizing the effectiveness of phase-sweeping for initial access and the comparative performance of different WPT techniques. Through these visualizations and analyses, the video provides a comprehensive understanding of WPT strategies and their practical implications in a RadioWeaves system.

6.6 Conclusion

The demonstrator showcases methods for powering ENDs wirelessly, addressing the initial access challenge and validating WPT strategies. Results confirm the feasibility of powering devices efficiently through distributed antennas, highlighting the synergy of random-phase, geometry-based, and reciprocity-based techniques in different scenarios.

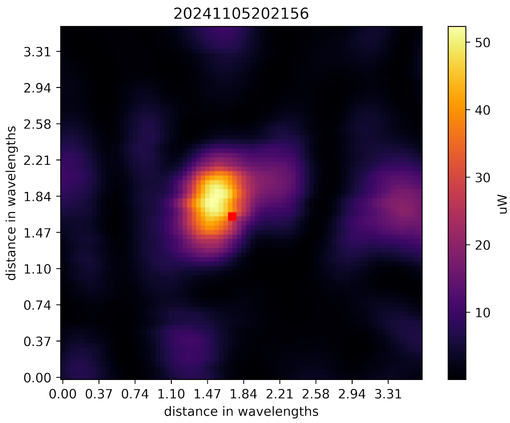

(a) Reciprocity-based beamforming

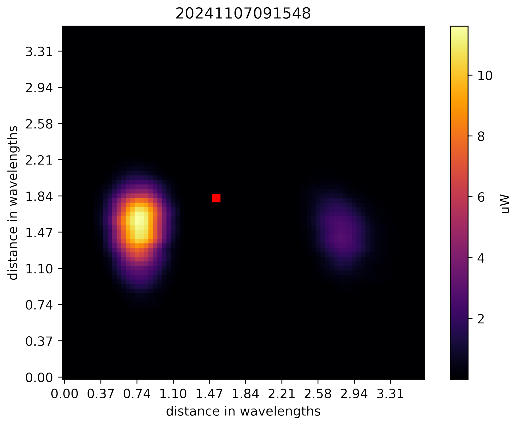

(b) LoS geometry-based beamforming

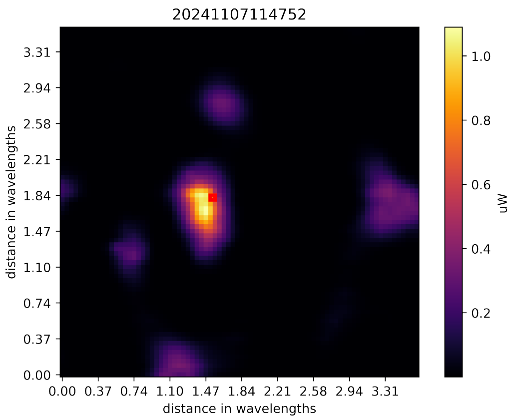

(c) First order reflections geometry-based beamforming

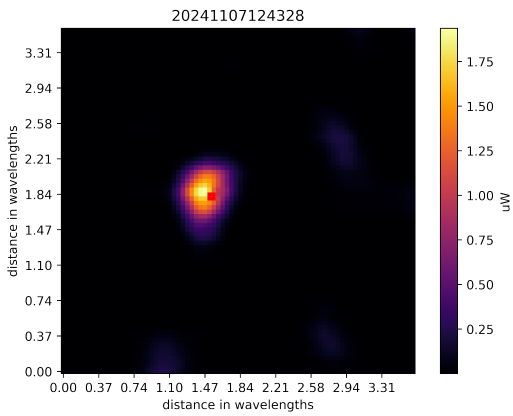

(d) Second order reflection geometry-based beamforming

Figure 6.2: Heatmaps of the received DC power for different WPT strategies. The target location is highlighted by the red rectangle.

6.7 References

Submitted and published studies are:

- J. Van Mulders, B. J. B. Deutschmann, G. Ottoy, L. De Strycker, L. Van der Perre, T. Wilding, and G. Callebaut, "Single versus Multi-Tone Wireless Power Transfer with Physically Large Arrays," in *2024 1st International Workshop on Energy Neutral and Sustainable IoT Devices and Infrastructure (EN-IoT 2024)*, Paris, France, Oct. 2024, p. 5.98 [29]
- G. Callebaut, J. Van Mulders, B. Cox, B. J. B. Deutschmann, G. Ottoy, L. De Strycker, and L. Van der Perre, "Experimental Study on the Effect of Synchronization Accuracy for Near-Field RF Wireless Power Transfer in Multi-Antenna Systems," in *2025 19th European Conference on Antennas and Propagation (EuCAP) (EuCAP 2025)*, Stockholm, Sweden, Mar. 2025, p. 4.98 [30]
- Position-based Wireless Power Transfer for Distributed XL-MIMO *(under development; initial results in [27]).*

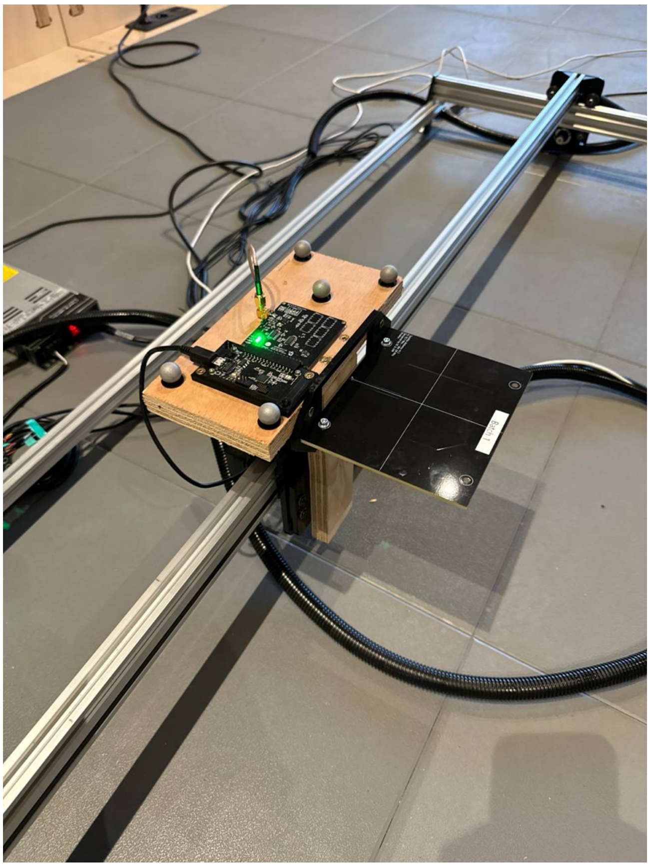

Figure 6.3: Energy Profiler mounted on our sampler machine in Techtile.

Chapter 7

Experiment 4b. Communicating with energy-neutral devices

7.1 Description

This experiment campaign shows the communication uplink from an END with bistatic, carrier suppression backscattering in the Techtile testbed. Backscatter communication is a wireless communication technique that enables devices to communicate by reflecting or modulating existing RF signals instead of generating their own signals. It demonstrates how the generation of a power spot can enable backscatter communication in near field and shows the influence of the distance on the bit error rate (BER).

7.2 Aim of the Demonstrator

This demonstrator has three main objectives. It first introduces the backscatter device. This low complex, energy-efficient and cheap uplink communicator was developed and is based on a simple microcontroller, an rf switch and an antenna Section 7.7. The second objective is touplink backscatter communication from an END when a power spot is generated at the END. We chose on-off keying (OOK) as a modulation technique as this is the least hardware and thus power demanding. The last goal of this demonstrator is to deliberate over experimental results showing the utility of carrier suppression bistatic backscattering in indoor environments.

7.3 Takeaway Points

The Backscatter Device: This refined hardware module only consists of a microcontroller, RF-switch and antenna. The microcontroller enables to send out any desired data in any wished-for encoding. Carrier suppression is achieved by using two timers to generate the signal and a local oscillator frequency.
Backscatter Communication: A local oscillator shifts the data signal away from the carrier signal, enabling carrier suppression with OOK modulation.

7.4 Challenges and Solutions

Backscattering with a single carrier wave generator has a limited range. With the generation of a power spot at the backscatter device, the received power and thus backscattered signal power is increased, making it possible to detect the backscattered data signal from a larger distance. Although OOK is fairly easy to implement on the transmitter side, this modulation technique is fairly susceptible to noise and clock drift. The chosen method shifts the necessary processing power for (de)modulation from the END to the Techtile testbed, enabling low power uplink communication.

7.5 Experimental results

The REINDEER consortium demonstrated bistatic, carrier suppressed uplink backscatter communication with low-complex, -power and cost effective hardware within the Techtile testbed. A visual representation of the test-setup and the backscatter device are depicted in Section 7.7.

7.6 Video Description

The video illustrates the bistatic backscatter set-up and introduces the different hardware components. A closer look is given on the backscatter device and its components. This is followed by a visualization of how a power spot is generated at the device location with the help of a heat map that shows the received power as generated in Chapter 6. In the next phase, the signal demodulation steps are explained and illustrated with some examples, highlighting the advantages of the backscatter uplink when a power spot is generated.

7.7 Conclusion

OOK based backscattering with carrier suppression when an backscatter device is positioned in a power spot is shown, overcoming the reduced data ranges present in SISO systems.

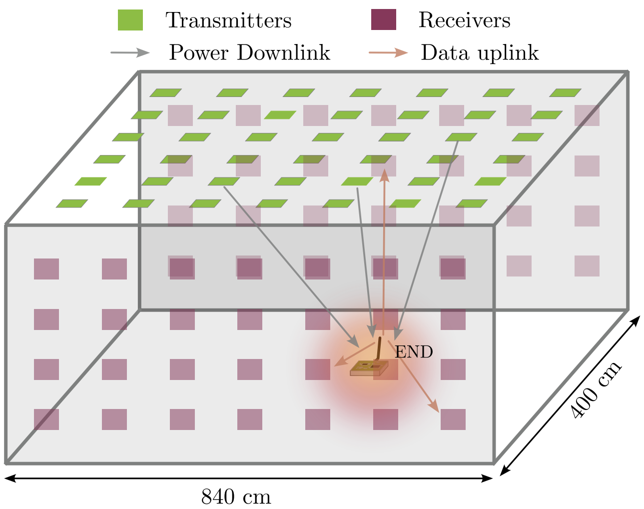

(a) Techtile Bistatic backscatter setup.

(b) Backscatter device (END)

Figure 7.1: Measurement setup and in housed developed backscatter device for the bistatic backscatter uplink.

Chapter 8

Experiment 4c. Positioning of energy-neutral device (END)

Knowing the actual position of an END holds large potential from an application point-of-view. Real-time location data can improve safety, performance, experience, and convenience in different types of solutions. Positioning is susceptible to the initial access problem. Before positioning, ENDs need to be powered and have to communicate, *e.g.*, through uplink pilot transmission. In this experiment, the *closed loop approach* elaborated in D4.2 [31] is experimentally evaluated.

Results from the first step in this closed loop approach can provide useful information on the uniformity of the power density throughout the experimental setup when random phase errors are introduced on purpose to each antenna element. In the next steps, the concept is to test different positioning algorithms based on pilot signals that can be generated with energy efficient backscattering communication. The positioning algorithms will be processed on the infrastructure side, to fully unburden the END. The Euclidean distances on a multitude of locations gives a good measure of how well the tested algorithms perform. In addition, we obtain insight into the influence of the amount of closed-loop iterations to for the estimated position to converge to a stable estimate in a simulation scenario, as well as the achievable error after convergence. With the envisioned communication setup in the Techtile infrastructure, the influence of the number of active antenna elements (receive and transmit) used for localization can be tested. The result of these tests can compare the received energy before and after the power spot generation. Power spot widening and END tracking could be implemented and tested at a later measurement stage.

Furthermore, the environment will also have a strong influence on the achievable positioning accuracy, especially at locations when the channel is in OLoS or non-line-of-sight (NLoS) condition. Another limiting factor is the large “two-way” path loss (PL) incurring with backscatter-based END that may put the receive-side infrastructure in a severely low input SNR regime. This will likewise severely impact the efficiency of a reciprocity-based beamformer. Using our direct-SLAM approach [27], we demonstrate that we can achieve a planar positioning RMSE of around $6.5\,\mathrm{cm}$ despite an SNR $\leq -6\,\mathrm{dB}$ and severe OLoS conditions. This is possible by learning the environment geometry, i.e., the locations and orientations of walls. Based on these learned environment parameters, positioning of the END in OLoS conditions is possible via NLoS multipath components that are reflected off these walls.

Chapter 9

Experiment 5. Multi-user capabilities

9.1 Description

The video demonstrates the increased user multiplexing performance achieved when distributing CSPs throughout a room under a dense user deployment. The experiment has been performed in a real room, within an office environment, by measuring the physical propagation channels between a set of closely spaced users and a set of distributed CSPs. To this end, a LunCH channel sounder has been employed, consisting of 4 distributed CSPs, and different scenarios have been analyzed to draw general conclusions on the multiuser capabilities of such a system.

9.2 Aim of the Demonstrator

- Introduce the LunCH channel sounder employed in this experiment.
- Illustrate the measurement scenarios analyzed in this experiment.
- Summarize the main findings of this research in terms of spatial multiplexing capabilities.

9.3 Video Description

The video will start with a recording of the LunCH channel sounder employed for in this experiment. In this case, it is a D-MIMO channel sounder with 4 distributed CSPs and each CSP is equipped with 2 panels consisting of 16 dual-polarized antennas in total. The main characteristics of the channel sounder, as well as the specific parameters considered in this experiment, will be animated into the corresponding scene. Some photos of the CSP distribution and the specific user deployments measured in the experiment, as well as an upper view schematic of the general setting will be then appear. Figure 9.1 shows such an example. Finally, the measured singular value spread (SVS), dirty-paper coding (DPC) and ZF multi-user sum-rates with different total number of antennas and CSP topologies are shown in the video, followed by the key findings of this work will be included.

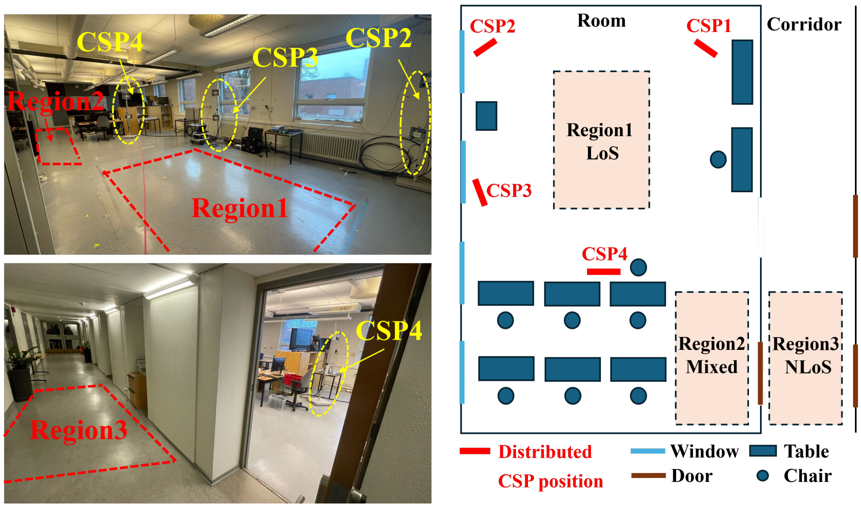

(a) (b)

Figure 9.1: (a) Photos of the measurement environments and (b) a schematic of the measurement regions.

Chapter 10

Conclusion

This report outlines the structure and purpose of D5.2, i.e., *Demonstrations of smart connectivity platform, support for resilient applications, and novel technologies*.

The following conclusions and takeaways points are made in the series of experiments (D5.3) and demonstration videos:

- The trade-offs between energy consumption, throughput, and user performance under varying topologies and precoding strategies is presented in experiment 1. This is done by grouping infrastructure resources tailored to the current conditions.
- There is a non-trivial trade-off between the robustness and latency when changing the number of contact service points (CSPs) in service. In experiment 2, an in-door scenario for design space exploration to find the number of CSPs that balances robustness and latency is illustrated using real-life hardware parameters from LuLIS.
- Demonstration of the capabilities of physically large array when it comes to positioning of single antenna devices and environmental learning. (Experiment 3)
- Demonstration of methods for powering energy-neutral devices (ENDs) wirelessly, addressing the initial access challenge and validating wireless power transfer (WPT) strategies. Results confirm the feasibility of powering devices efficiently through distributed antennas, highlighting the synergy of random-phase, geometry-based, and reciprocity-based techniques in different scenarios. (Experiment 4a)
- Demonstration of real-time uplink backscatter communication from an END when a power spot is generated at the END. (Experiment 4b)
- Knowing the actual position of an END holds large potential from an application point-of-view. Real-time location data can improve safety, performance, experience, and convenience in different types of solutions. (Experiment 4c)
- Compared with co-located CSP setup, the distributed CSP set up is demonstrated to provide better user separability in an in-door lab environment. (Experiment 5)

The findings and conclusions in the experiments provide new insights in the development of cell-free and RadioWeaves systems. In REINDEER, some capabilities are demonstrated in real-life hardware and hardware-fed simulations. On top of that, our experiments and demonstration videos show the importance of these investigations and the current gaps to make those next-generation systems a reality. By creating these scientific demonstration videos, both the broader audience and the science community is aware of this research and the challenges ahead.

Bibliography

[1] H. Choi, J. Oh, J. Chung, G. C. Alexandropoulos, and J. Choi, "WiThRay: A Versatile Ray-Tracing Simulator for Smart Wireless Environments," *Access*, 2023.

[2] O. Authors, "QuaDRiGa: A 3-D Multi-Cell Channel Model With Time Evolution for Enabling Virtual Field Trials," *Transactions on Antennas and Propagation*, Year.

[3] Y. He, Y. Zhang, J. Zhang, L. Pang, Y. Chen, and G. Ren, "Investigation and Comparison of QuaDRiGa, NYUSIM and MG5G Channel Models for 5G Wireless Communications," 2020.

[4] J. Hoydis, F. A. Aoudia, S. Cammerer, *et al.*, "Sionna RT: Differentiable Ray Tracing for Radio Propagation Modeling," *arXiv preprint arXiv:2303.11103*, 2023.

[5] W. Tärneberg, A. Fedorov, G. Callebaut, L. Van der Perre, and E. Fitzgerald, "Towards Practical Cell-Free 6G Network Deployments: An Open-Source End-to-End Ray Tracing Simulator," in *2023 57th Asilomar Conference on Signals, Systems, and Computers*, 2023, pp. 1000–1005. DOI: 10.1109/IEEECONF59524.2023.10476998.

[6] J. Karedal, N. Czink, A. Paier, F. Tufvesson, and A. F. Molisch, "A Geometry-Based Stochastic MIMO Model for Vehicle-to-Vehicle Communications," *Transactions on Vehicular Technology*, 2011.

[7] V.-M. Kolmonen, M. Vehkapera, T. Jamsa, and A. F. Molisch, "Evaluation of the Spatial Consistency Feature in the 3GPP Geometry-Based Stochastic Channel Model," *Transactions on Antennas and Propagation*, 2011.

[8] C.-X. Wang, X. Cheng, D. I. Laurenson, S. Salous, and A. V. Vasilakos, "A Geometry-Based Stochastic Channel Model for MIMO Mobile-to-Mobile Communications," *Transactions on Vehicular Technology*, 2008.

[9] V. Degli-Esposti, F. Fuschini, E. M. Vitucci, and G. Falciasecca, "Ray Tracing for Radio Propagation Modeling: Principles and Applications," *Access*, 2015.

[10] J. Smith and E. Johnson, "Exhaustive Ray Tracing for 6G Topics such as RIS or Integrated Sensing and Communications," *Journal of Advanced Communications*, 2022.

[11] T. Keymeulen, "High-Level Simulator of Federation Orchestration," M.S. thesis, Lund University, 2022.

[12] M. Beke, "Dynamic Update of CSP Allocations in Federation Orchestration," M.S. thesis, Lund University, Department of Electrical and Information Technology, 2024.

[13] "Techtile–open 6g r&d testbed for communication, positioning, sensing, wpt and federated learning."

[14] R. project, "Detailed experimental validation plan, design of experiments, and definition of common formats," REINDEER project, Deliverable ICT-52-2020 / D5.1, 2023.

[15] C. Nelson, X. Li, A. Fedorov, B. Deutschmann, and F. Tufvesson, "Distributed MIMO Measurements for Integrated Communication and Sensing in an Industrial Environment," *Sensors*, vol. 24, no. 5, p. 1385, Feb. 2024, ISSN: 1424-8220. DOI: 10.3390/s24051385. [Online]. Available: http://dx.doi.org/10.3390/s24051385.

[16] M. Sandra, C. Nelson, X. Li, X. Cai, F. Tufvesson, and A. J. Johansson, *A Wideband Distributed Massive MIMO Channel Sounder for Communication and Sensing*, 2024. arXiv: 2403.11856 [eess.SP]. [Online]. Available: https://arxiv.org/abs/2403.11856.

[17] C. Nelson, X. Li, T. Wilding, B. Deutschmann, K. Witrisal, and F. Tufvesson, "Large Intelligent Surface Measurements for Joint Communication and Sensing," *arXiv preprint arXiv:2304.12457*, pp. 228–233, 2023. DOI: 10.1109/EuCNC/6GSummit58263.2023.10188339.

[18] G. Callebaut, L. Liu, T. Eriksson, L. Van der Perre, O. Edfors, and C. Fager, "6G Radio Testbeds: Requirements, Trends, and Approaches," *IEEE Microwave Magazine*, vol. 25, no. 4, pp. 14–31, 2024. DOI: 10.1109/MMM.2024.3351970.

[19] O. T. Demir, L. Méndez-Monsanto, N. Bastianello, E. Fitzgerald, and G. Callebaut, "Energy Reduction in Cell-Free Massive MIMO through Fine-Grained Resource Management," in *2024 Joint European Conference on Networks and Communications & 6G Summit (EuCNC/6G Summit)*, 2024, pp. 547–552. DOI: 10.1109/EuCNC/6GSummit60053.2024.10597081.

[20] O. Edfors, R. Brazil, H. Petautschnig, G. Callebaut, T. Feys, L. V. der Perre, E. G. Larsson, O. Edfors, E. Fitzgerald, L. Liu, J. R. Sanchez, W. Tärneberg, P. Frenger, B. Deutschmann, T. Wilding, and K. Witrisal, "Initial assessment of architectures and hardware resources for a RadioWeaves infrastructure, Reindeer deliverable D2.1," Deliverable, version 1, Jan. 2022. DOI: 10.5281/zenodo.5938909. [Online]. Available: https://doi.org/10.5281/zenodo.5938909.

[21] "Evaluation of the distribution of processing across infrastructure and associated requirements on back-haul and synchronization, Reindeer deliverable D2.2," Deliverable, version 1, 2023.

[22] L. Tinnerberg, D. Iancu, O. Edfors, L. Liu, and J. V. Alegría, *Spectrum efficiency and processing latency trade-offs in panel-based lis*, 2024. arXiv: 2411.19147 [eess.SP]. [Online]. Available: https://arxiv.org/abs/2411.19147.

[23] A. Fascista, B. J. B. Deutschmann, M. F. Keskin, T. Wilding, A. Coluccia, K. Witrisal, E. Leitinger, G. Seco-Granados, and H. Wymeersch, *Joint Localization, Synchronization and Mapping via Phase-Coherent Distributed Arrays*, 2024. arXiv: 2409.12478 [eess.SP]. [Online]. Available: https://arxiv.org/abs/2409.12478.

[24] R. project, "Position Estimation and Environment Learning," REINDEER project, Deliverable ICT-52-2020 / D3.3, 2023.

[25] B. J. B. Deutschmann, C. Nelson, M. Henriksson, G. Marti, A. Kosasih, N. Tervo, E. Leitinger, and F. Tufvesson, "Accurate Direct Positioning in Distributed MIMO Using Delay-Doppler Channel Measurements," in *2024 IEEE 25th International Workshop on Signal Processing Advances in Wireless Communications (SPAWC) (IEEE SPAWC 2024)*, Lucca, Italy, Sep. 2024, p. 5.

[26] R. project, "Ultra-robust and low-latency communications and mobility support," REINDEER project, Deliverable (unpublished) ICT-52-2020 / D3.4, 2024.

[27] R. project, "Validation of concepts and experimental assessment of key technologies," REINDEER project, Deliverable ICT-52-2020 / D5.3, 2024.

[28] European Telecommunications Standards Institute (ETSI), "ETSI TS 138 101," ETSI, Technical Specification, Jan. 2023.

[29] J. Van Mulders, B. J. B. Deutschmann, G. Ottoy, L. De Strycker, L. Van der Perre, T. Wilding, and G. Callebaut, "Single versus Multi-Tone Wireless Power Transfer with Physically Large Arrays," in *2024 1st International Workshop on Energy Neutral and Sustainable IoT Devices and Infrastructure (EN-IoT 2024)*, Paris, France, Oct. 2024, p. 5.98.

[30] G. Callebaut, J. Van Mulders, B. Cox, B. J. B. Deutschmann, G. Ottoy, L. De Strycker, and L. Van der Perre, "Experimental Study on the Effect of Synchronization Accuracy for Near-Field RF Wireless Power Transfer in Multi-Antenna Systems," in *2025 19th European Conference on Antennas and Propagation (EuCAP) (EuCAP 2025)*, Stockholm, Sweden, Mar. 2025, p. 4.98.

[31] R. project, "Signal processing for WPT and uplink signalling, exploiting environment awareness," REINDEER project, Deliverable ICT-52-2020 / D4.2, 2023.